Title

Correlated Protein Environments Drive Quantum Coherence Lifetimes in Photosynthetic Pigment-Protein Complexes

Journal

Chem, 4(1)

ISSN

1925-6981

Authors

Rolczynski, Brian S
Zheng, Haibin
Singh, Ved P
et al.

Publication Date

2018

DOI

10.1016/j.chempr.2017.12.009

Peer reviewed

Chem

CellPress

Article

Correlated Protein Environments Drive Quantum Coherence Lifetimes in Photosynthetic Pigment-Protein Complexes

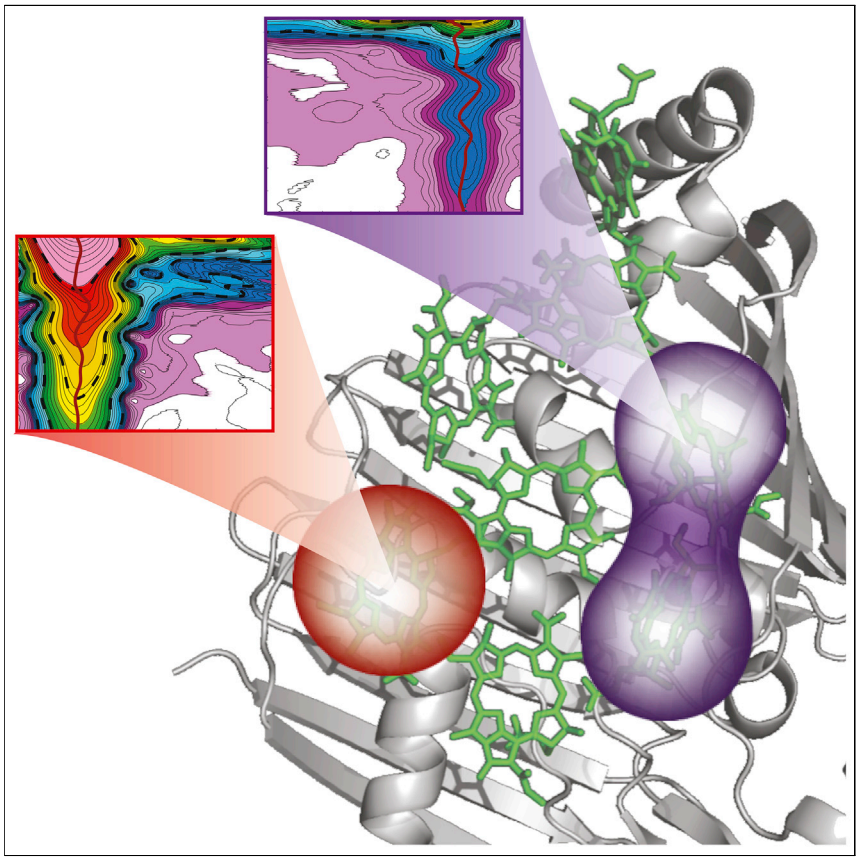

Energy transfer in photosynthesis occurs as electronic excitations of coupled chromophores interact with their environment. The microscopic nature of these motions can enable novel energy-transfer mechanisms if the motions are not random. This study reveals synchronized and correlated fluctuations of the states within a photosynthetic pigment-protein complex, which explains prior observations of long-lived quantum coherence.

Brian S. Rolczynski, Haibin Zheng, Ved P. Singh, ..., Sabre Kais, Richard J. Cogdell, Gregory S. Engel

gsengel@uchicago.edu

HIGHLIGHTS

Method of observing spectral motions directly after femtosecond excitation

Observed synchronized fluctuations among electronic states in a protein complex

Observed correlated spectral motion between occupied and unoccupied excited states

Rolczynski et al., Chem 4, 138–149
January 11, 2018
https://doi.org/10.1016/j.chempr.2017.12.009

Chem

CellPress

Article

Correlated Protein Environments Drive Quantum Coherence Lifetimes in Photosynthetic Pigment-Protein Complexes

Brian S. Rolczynski,[1] Haibin Zheng,[1] Ved P. Singh,[1,5] Polina Navotnaya,[1] Alan R. Ginzburg,[1] Justin R. Caram,[1,6] Khuram Ashraf,[2,7] Alastair T. Gardiner,[2] Shu-Hao Yeh,[1,3] Sabre Kais,[3,4] Richard J. Cogdell,[2] and Gregory S. Engel[1,8,*]

SUMMARY

Early reports of long-lived quantum beating signals in photosynthetic pigment-protein complexes were interpreted to suggest that electronic coherence benefits from protection by the protein, but many subsequent studies have suggested instead that vibrational or vibronic contributions are responsible for the observed signals. Here, we devised two 2D-spectroscopy methods to observe how each exciton is perturbed by its nuclear environment in a photosynthetic complex. The first approach simultaneously monitors each exciton's energy fluctuations over time to obtain its time-dependent electronic-nuclear interactions. The second method isolates evidence of coupled interexcitonic environmental motions. The techniques are validated with Nile Blue A and subsequently used on the Fenna-Matthews-Olson (FMO) complex. The FMO data reveal that each exciton experiences nearly identical spectral motion after excitation and that spectral motion of one excited exciton induces similar motion on unpopulated neighboring excitonic states. These synchronized and correlated spectral dynamics prolong coherences in the FMO complex after femtosecond excitation.

INTRODUCTION

Photosynthesis depends on efficient electronic energy transfer through an array of pigment-protein complexes.[1] Energy transfer requires perturbations from the environment, and the dephasing of coherent states generated within the system provides a sensitive probe of these dynamics.[2–6] Dephasing occurs when a sample ensemble prepared in a coherent state is subject to random environmental perturbations.[7] In general, dephasing can be slowed by reducing the temperature or physically separating the coherent states from their environments,[8] but protein complexes *in vivo* cannot use either of these approaches. Nonetheless, some photosynthetic pigment-protein complexes display long-lived coherences, even at physiologic temperatures.[9] Microscopically, it has been hypothesized that correlated motions within the protein may explain this long-lived coherence.[10]

Quantum coherences persisting on the timescale of energy transfer have been measured, leading to proposals that these systems enlist quantum dynamics to enhance their energy transport efficiencies.[2,11–16] More recent works suggest instead that the coherence signals result from the following: (1) pure vibrational states,[17–19] (2) vibronic (mixed electronic-vibrational) states,[20–22] or (3) pure electronic states experiencing correlated nuclear environments and/or non-Markovian

The Bigger Picture

Observations of quantum coherence in photosynthetic complexes spawned a new field of quantum biology for the study of how biology exploits quantum dynamics. However, theoretical models have suggested that these signals may not arise from electronic dynamics but rather from simple molecular vibrations. The key question is whether different excited electronic states evolve in a correlated fashion after excitation.

Here, we have developed two spectroscopic methods to provide experimental evidence that electronic states within a photosynthetic protein-pigment complex experience correlated fluctuations after excitation. Surprisingly, we found that the excitonic transitions in the Fenna-Matthews-Olson complex all undergo the same spectral motion after excitation despite having different degrees of delocalization and different local environments, etc. Such correlated spectral motion explains how quantum coherence among electronic states can persist for so long after femtosecond excitation.

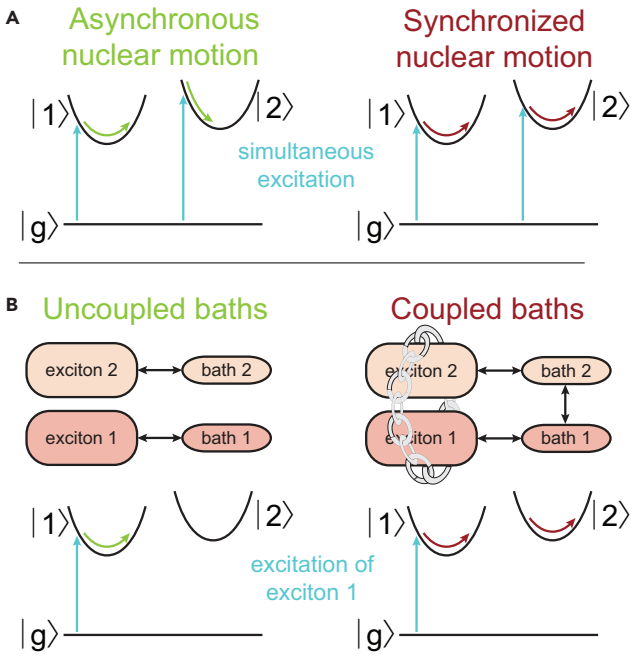

Figure 1. Photogenerated Excited States Interact with Their Respective Baths, which Permit Energy Dissipation and Generate Spectral Diffusion

Both of these processes induce dephasing. However, synchronous or correlated nuclear effects, measurable by 2D-STEPS and 2D-TRIPS, can increase coherence lifetimes.

(A) Unsynchronized motion occurs when the nuclear motions propagate differently for distinct excited states. Synchronized spectral motion among excitons ensures that their phases propagate together, because energy fluctuations on one exciton are experienced by the other excitons as well. Such fluctuations do not contribute to phase evolution mismatch between excitons.

(B) Coupling between the baths of two distinct excitons causes correlated spectral motion to occur in the electronic states, preserving their phase relationship longer, even when only one of the excitons is excited.

vibrational perturbations.[5,23–26] Subtle details of these electronic-nuclear interactions govern the observed quantum dynamics.

Here, we extract information from the third-order nonlinear response of the system by using two approaches: 2D single-time-domain exciton perturbation spectroscopy (2D-STEPS) and 2D time-resolved interexciton perturbation spectroscopy (2D-TRIPS). These optical, time-domain spectroscopies probe vibrational motion by examining correlated dynamics of each exciton's spectral motion. 2D-STEPS measures how excited-state nuclear motions systematically perturb individual excitonic transitions after excitation, whereas 2D-TRIPS probes how nuclear motions spawned by exciting one exciton affect other unoccupied excitonic states (Figure 1). In both approaches, three optical pulses are incident on the sample, resulting in a third-order signal. The 1–2, 2–3, and 3-signal pulse pairs are separated by the coherence (τ), waiting time (T), and rephasing time (t), respectively. The first pulse creates a quantum coherence $|g\rangle\langle e_i|$ between the i^{th} exciton and ground states, and also launches a wavepacket from the Franck-Condon position on the excited-state surface.[27] These coherences propagate according to $\exp(-iH_g\tau/h)|g\rangle\langle e_i|\exp(iH_{e_i}\tau/h)$ and the mismatch between H_{e_i} and H_g causes the system to evolve phase at the frequency $\omega_{ei,g} = \omega_{ei} - \omega_g$.[7] The nuclear motions meanwhile perturb the corresponding excited-state transitions, causing $\omega_{ei,g}$ to fluctuate over time.[27] If individual complexes within the ensemble experience

[1]Department of Chemistry, Institute for Biophysical Dynamics and James Franck Institute, University of Chicago, Chicago, IL, USA

[2]Institute of Biomedical and Life Sciences, Glasgow Biomedical Research Centre, University of Glasgow, Glasgow, UK

[3]Qatar Environment and Energy Research Institute, Hamad Bin Khalifa University, Qatar Foundation, Doha, Qatar

[4]Department of Chemistry, Purdue University, West Lafayette, IN, USA

[5]Present address: Janelia Research Campus, Ashburn, VA 20147, USA

[6]Present address: Department of Chemistry and Biochemistry, University of California, Los Angeles, Los Angeles, CA, USA

[7]Present address: Department of Physiology and Cellular Biophysics, Columbia University, New York, NY, USA

[8]Lead Contact

*Correspondence: gsengel@uchicago.edu

https://doi.org/10.1016/j.chempr.2017.12.009

distinct perturbations, they will dephase. In contrast, systematic or synchronized motions of the excited-state energy gap will be detected.

After this initial excitation, two subsequent pulses reverse the phase evolution of the system.[7] The system once again evolves phase in the *t* domain, with a phase velocity determined by the difference of the states' frequencies involved in the coherences. 2D-STEPS measures the dependence of ω_τ on τ to find the vibrational dynamics by using the ω_t domain to sort the contributions from each exciton. This spectroscopy is sensitive only to dynamics on the excited-state surface. (For further discussion, see Figure 4 and Spectroscopy Overview.)

In 2D-TRIPS, this time dependence is examined in both the τ and *t* domains. The nuclear motions of a chosen exciton *i* propagate for a duration τ' in the τ domain, then the spectral motions of a distinct exciton $j \neq i$ are observed in the *t* domain. As τ' advances, the effect on the spectral motion in *t* is observed. Dependencies observed between these two excitons indicate correlations between their nuclear environments.

In this report, first the short-time Fourier-transform approach is validated with Nile Blue A as a model system. Subsequently, it is used on the Fenna-Matthews-Olson (FMO) complex of *Chlorobaculum tepidum*, which is known to exhibit long-lived coherences even at physiologic temperatures.[9,12] FMO contains seven coupled bacteriochlorophyll *a* (BChl *a*) chromophores in a hydrophobic pocket, plus an eighth more weakly bound BChl *a* just outside the pocket, which functionally links the complex to the Chlorosome baseplate.[28] Coupling among these sites leads to several different excitonic states.[29] Their nuclei also provide an array of vibrational modes,[30] which couple to the electronic states to produce dephasing.[7]

RESULTS

The frequency evolution of the electronic state populations of FMO were analyzed by 2D-STEPS, as described in the Experimental Procedures. The signal is dominated by intense peaks near the selected ω_t frequencies and evolves over τ' (Figure 2). The distinct exciton peaks in these spectrograms exhibit synchronized spectral motions, which are reproducible in repeated experiments (Figures S6–S10). The power spectral densities of these peak motions contain frequency components at approximately 40, 120, 185, and 300 cm^{-1}, which agree with vibrational frequencies of 46, 117, 167–202, and 284–291 cm^{-1}, respectively, reported with fluorescence line-narrowing measurements of FMO.[30] The frequency components of this spectral motion have been assigned to intramolecular vibrational modes within the chromophores, although the 40 cm^{-1} feature has been attributed either to phonon modes or vibrations of BChl *a*'s acetyl tail.[31–34] Because the coherence time domain only accesses coherent superpositions of vibrational states on the excited-state surface (see the Experimental Procedure for further discussion), these frequency fluctuations are attributed to the excited-state vibrational motions. As a result of their delocalization, phonon modes may have an impact on the excitons collectively; but local vibrational motions should not. We therefore attribute the clear synchronized spectral motion to local modes acting independently on the seven BChl *a* chromophores to produce synchronized motions for the distinct excitons. For reference, the same treatment was applied to a Nile Blue A standard, confirming that it produces its own expected power spectral densities,[35–38] which are distinct from those in FMO. For a more detailed discussion of these Nile Blue A experiments, including narrower spectrogram windows and distinct waiting times, refer to Section S9 in the Supplemental Information.

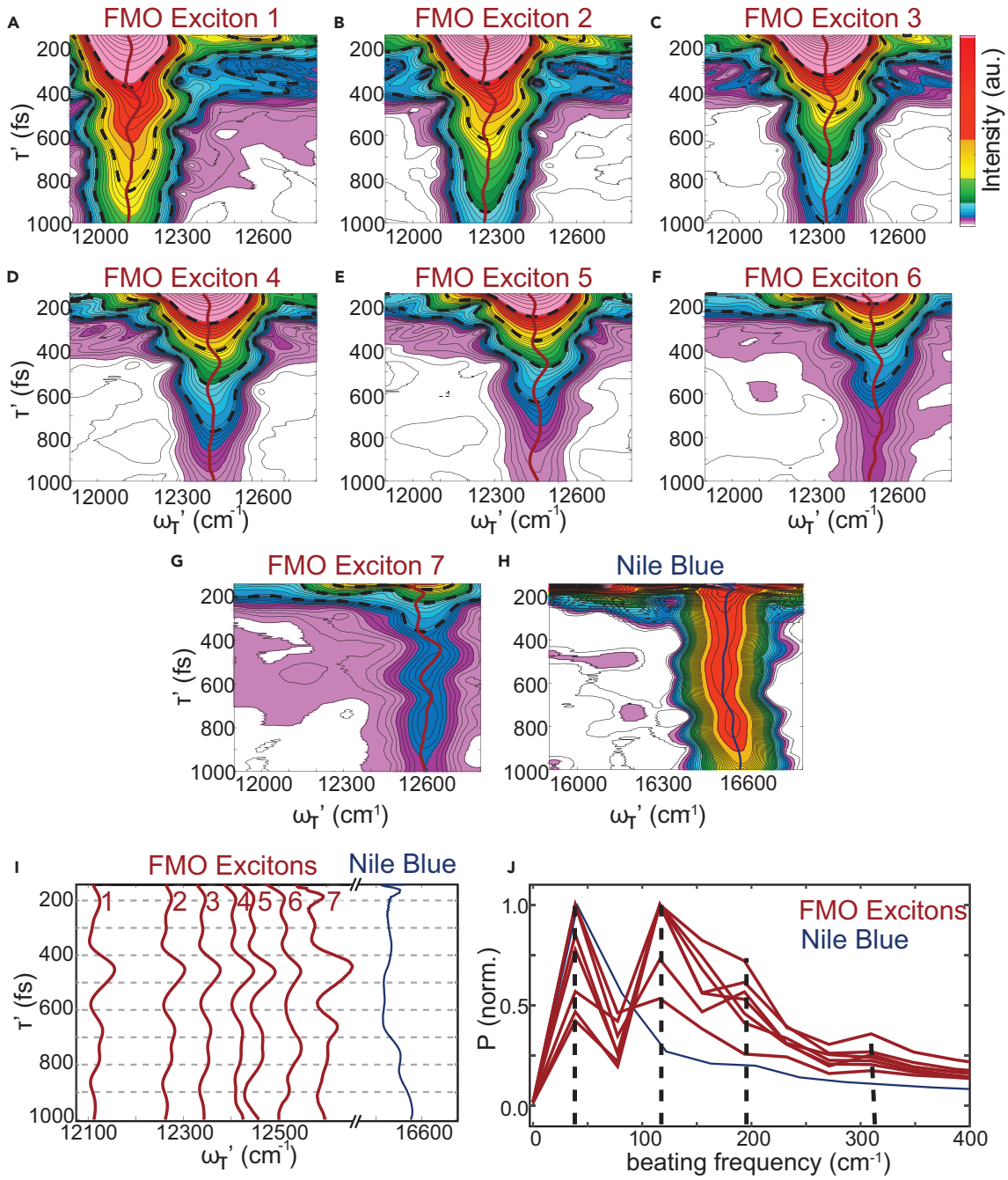

Figure 2. The Spectral Motion of Distinct Excitons Is Synchronized

(A–H) 2D-STEPS spectrograms are shown for (A–G) excitons 1–7 of FMO and (H) Nile Blue A. The oscillating red and blue lines indicate the peak position for each τ' in the FMO and Nile Blue A spectra, respectively.

(I) The peak oscillations in (A)–(H) are plotted together.

(J) The power spectral densities obtained from the peak fluctuations are plotted together, yielding peaks at 40, 120, 200, and 300 cm^{-1} for FMO. The peak fluctuations and power spectral density for Nile Blue A are different from those for FMO.

See also Figures S1–S10, S12, and S15 and Table S1.

2D-TRIPS uses a similar strategy to 2D-STEPS. However, 2D-TRIPS exploits multiple time domains to isolate evidence of interexcitonic vibrational motion during the coherence time and a subsequent time period. Using a time-ordered pulse

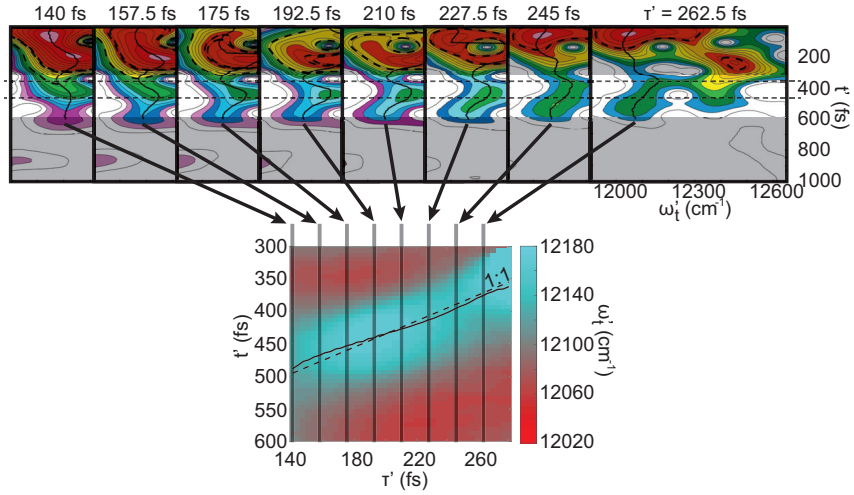

Figure 3. 2D-TRIPS Spectrograms Are Obtained for Excitons 1 and 7 in the Coherence and Rephasing Domains, Respectively

(Top) Representative spectrograms are shown for systematically varying τ'. The horizontal dotted lines highlight the shift of the second oscillation in t' as τ' increases.

(Bottom) The second frequency fluctuation cycle is shown in a heatmap. The vertical, transparent black lines indicate where the representative slices from the top of the figure contribute to the heatmap. The solid black line indicates the shifting t' position as a function of τ', whereas the dotted line shows a slope of −1 for comparison. The slope is negative because the t' axis is reversed. See also Figures S1, S3, and S9–S11.

sequence, we observe how propagation of one exciton's nuclear motions during the coherence time affects those of another exciton during the rephasing time. Because of its smaller time-domain range, the frequency resolution is lower in the short-time Fourier transform than in the standard Fourier transform. Therefore, exciton signals that are too close in energy overlap spectrally, and this overlap obscures their distinct contributions. We therefore focus primarily on excitons 1 and 7 for this analysis, because their energies are separated by approximately 500 cm^{-1} (other combinations are shown in Figure S11). Exciton 7 is selected in the τ domain and allowed to propagate for a designated duration τ'. Subsequently, the t domain spectrogram is obtained, and its exciton 1 cross-peak fluctuations are observed as a function of both τ' and t'. This process is repeated with systematic variation of τ', to observe any dependence of the spectral fluctuations in t' on τ'. For uncorrelated nuclear environments, no dependence would be observed.

Figure 3 displays 2D-TRIPS spectrograms for excitons 1 and 7. It resolves two peak fluctuation cycles occurring over the first 600 fs of t'. Although the first cycle fluctuates as expected when it is distinguishable (e.g., τ' = 140 and 157.5 fs), we do not focus on it here because inhomogeneous broadening contributions, which dominate the signal at low t',[7] contaminate the upper region of the spectrograms. However, the second fluctuation is well isolated and suitable for comparison with varying τ'. When τ' increases, the phase of the spectral motion in the rephasing domain shifts by a nearly equivalent increment, indicating that spectral motion during the coherence time advances the phase of spectral motion of a different exciton later in time. The dashed, horizontal lines in Figure 3 indicate the phase progression of this second cycle with increasing τ'. The heatmap in Figure 3 shows that the phase progression is maintained even for smaller increments of τ'. The solid black line in the heatmap indicates the peak position. A horizontal black line would have indicated no correlation of the peak energy between t and τ; however, this sloped line represents

a correlation of the nuclear phase between increasing τ and decreasing t. In essence, the vibrational motion in the rephasing domain inherits vibrational phase from the coherence time domain, although different excitons were excited in these two domains.

DISCUSSION

The 2D-STEPS spectrograms display synchronized spectral motion of the excitons over much of the first picosecond. Because these spectrograms report dynamics in the coherence time domain, when only single excitations are allowed, these motions indicate that the ensemble trajectory for each exciton independently undergoes very similar dynamics following its initial excitation. These similar vibrational motions occur despite the different site compositions of the excitons. The excitons are delocalized over a number of sites described by their inverse participation ratios, which span 1.28–2.54 in FMO.[39] As a result, some are nearly monomeric, while others are nearly trimeric. Furthermore, previous work has shown that vibrational modes arise from intermolecular coupling between bacteriochlorophylls.[19] Therefore, after excitation with a short laser pulse, a given exciton will exhibit synchronized nuclear motions across the ensemble;[40] but the motions of distinct excitons can diverge over time. It is therefore not a given that FMO's excited states would exhibit these synchronized vibrational oscillations over a picosecond. Nonetheless, the 2D-STEPS results indicate that the excitons experience synchronized nuclear perturbations over this duration.

Therefore, even before invoking particular effects, such as correlated nuclear environments, non-Markovian fluctuations, or vibronic states, when a coherent superposition of excited states is generated in 2D spectroscopy,[9,12] the excitons' spectral motion will remain synchronized over approximately the first picosecond because of their independently similar vibrational motions. Thus, in an ultrafast 2D experiment, electronic coherences may be prolonged in FMO as a result of synchronized nuclear fluctuations, even without invoking correlated nuclear environments, for suitably broadband coherent light capable of generating superpositions of electronic and vibrational excited states in FMO. This duration coincides with the relevant timescale for energy transfer in FMO,[9,11] and prolonged coherences have been reported to enhance transport efficiencies.[14,15]

In addition to this effect, the results from 2D-TRIPS indicate coupling between the nuclear motions of distinct excitons, suggesting an additional mechanism to enhance coherence lifetimes. These correlated interexcitonic nuclear environments increase the critical temperature for the transition of coherent-to-incoherent energy transport.[41] Coherences lasting hundreds of femtoseconds in FMO at room temperature have been observed previously,[9] which is consistent with this additional explanation. In terms of Redfield theory,[3] these correlated motions will reduce the nuclear damping. Coupling between numerous harmonic oscillators can also induce synchrony, so exploring whether this mechanism applies to the vibrational modes in FMO represents a promising future direction.[42,43]

After femtosecond excitation, the FMO complex exhibits both synchronized and correlated excitonic nuclear environments. 2D-STEPS reveals similar spectral motion for each exciton after femtosecond excitation so that, even before considering interexcitonic vibrational correlations, superpositions of these excitons propagate in common for at least 1 ps at 77 K. Furthermore, 2D-TRIPS provides direct evidence that one exciton's spectral motion affects a distinct exciton's nuclear dynamics.

These properties result from embedding multiple identical chromophores, with the same intramolecular vibrational modes, in close proximity within the protein scaffold. Taken together, these data provide three key insights into the origins of long-lived coherence in photosynthetic systems: first, the common response of the chromophores ensures that the excited state spectral motions will be synchronized after femtosecond excitation; second, estimating the spectral diffusion without subtracting the synchronized motion dramatically overestimates the system-bath coupling; third, nuclear motions on one exciton do affect the energy gap of other excitons, which will favor coherent energy-transfer mechanisms.[16,24,44] Thus, the structured nuclear environment within the photosynthetic antenna complex creates intricate and programmed spectral motion that drives energy-transfer dynamics.

EXPERIMENTAL PROCEDURES

Sample Preparation

FMO extraction was performed according to a published procedure.[45] According to another published procedure,[12] the extracted sample was then prepared in a 65/35 (v/v) glycerol/water mixture with a 800 mM Tris-HCl buffer (pH 8.0), 50 mM NaCl, and 0.1% lauryldimethylamineoxide detergent. For the spectroscopy, the sample was prepared at an optical density of approximately 0.3 at 12,450 cm^{-1} with a 200 μm path length and vitrified to 77 K with liquid nitrogen.

Nile Blue A was dissolved in water and sonicated for 20 min. Subsequently, it was filtered with a 0.2 μm syringe filter and mixed into a 65/35 glycerol/water mixture. It was prepared with an optical density of 0.3 at 15,750 cm^{-1} in a 200 μm pathlength and vitrified to 77 K in liquid nitrogen.

Experimental Parameters

The experiments were performed with a previously described spectrometer designed for the acquisition of 2D electronic spectra.[46] For FMO, the coherence and waiting times were sampled from −1,001 to 2,002 fs in 3.5 fs steps, and from 0 to 1,860 fs in 30 fs steps, respectively. Rephasing times were obtained interferometrically. The beam fluence was 640 $pW/\mu m^2$ in a 100 μm diameter spot for FMO. The local oscillator was attenuated by 10^4. The pulse width was 14 fs (fwhm), and the repetition rate was 5 kHz. (Further details are available in Section S10 of the Supplemental Information.)

For Nile Blue A, the coherence times were sampled from −1,001 to 2,002 fs in 2.6 fs steps, and the waiting times were obtained at 0, 30, 60, 150, 270, and 1,000 fs. For this system, the results at $T = 0$ fs are discussed here as a representative example, whereas the other waiting times appear in Section S9 of the Supplemental Information. Because fewer waiting times were used, three to six scans were measured at each waiting time and averaged. The fluence was 1.9 $nW/\mu m^2$.

Spectroscopy Overview

Three beams are incident on the sample in a boxcar geometry. The sub-ensemble that interacts with all three beams accumulates their momentum and emits a signal in the spatial direction that conserves momentum. Using a spatial mask, we therefore measure the signal from the sub-ensemble that interacts once with each beam. Within the density matrix formalism, and applying the rotating wave approximation, each of these interactions can promote or decrement either the ket or bra sides of the density matrix.[7] The sequences resulting from possible combinations of these interactions are called Liouville pathways and expressed in Feynman diagrams.

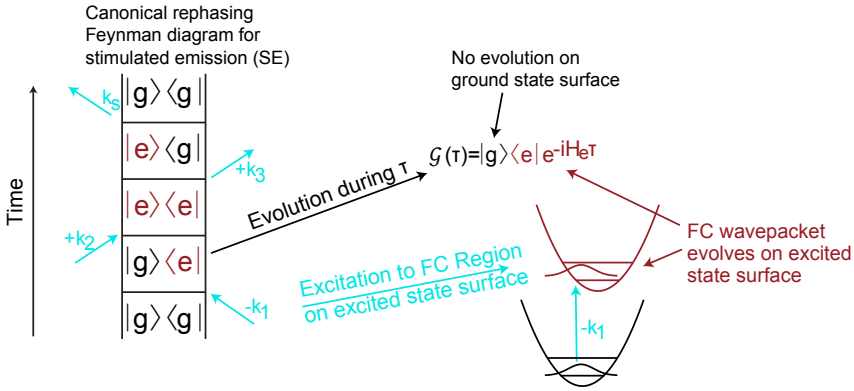

Figure 4. 2D-STEPS Measures Spectral Motion on the Excited State

After the first light-matter interaction, represented in this Liouville pathway by $-k_1$, a coherence is generated between the $|g\rangle$ and $\langle e|$ state manifolds, which evolves according to the Green's function $\mathcal{G}(\tau)$. The excited-state wave packet begins in the Franck-Condon region on the excited-state surface and propagates across the excited-state surface over time. However, the ground-state wave function does not propagate across the ground state because it is already at its equilibrium position. Therefore, within the coherence domain, the excited-state frequency described by H_e exhibits nuclear fluctuations, whereas the ground state does not. See also Figure S13.

Numerous works have tabulated all the Liouville pathways available in 2D electronic spectroscopy,[7,47,48] so this information is not reproduced here. Rather, Figure 4 uses a representative Feynman diagram to illustrate that the coherence domain encodes only nuclear motions on the excited-state surface during the coherence time, because of the evolution of the density matrix within the semiclassical formalism derived by Mukamel.[7] As discussed in the Results and Section S10 of the Supplemental Information, this principle is tested with Nile Blue A.

In the rephasing Liouville pathways ($\tau > 0$ fs), the 2D-STEPS signal arises after a configuration $|g\rangle\langle g|$ is promoted to $|g\rangle\langle e_i|$ from one light-matter interaction. As shown in Figure 4, in τ, the bra state is determined by the laser spectrum, whereas the ket side remains in the ground state. The laser bandwidth exceeds 1,000 cm^{-1} (Figure S1), so it is capable of exciting multiple vibrational levels within the excited-state manifold. Therefore, the spectral dynamics in the τ domain data reported here arise from evolution of nuclear motions on the excited-state surface.[27] This excited-state contribution is further discussed in the Results and Section S9 of the Supplemental Information.

In the 2D-TRIPS technique, again using rephasing signals and Liouville pathways, first the bra side is excited, causing the system's phase to evolve during τ. Subsequently, the ket side is excited and reverses that phase propagation during t. Importantly, these processes are occurring in the same individual complexes, which is enforced by the boxcar beam geometry and conservation of momentum. We elect to observe the spectral fluctuations of distinct excitons during these two time periods. In the absence of coupling between these two distinct excitonic environments, the spectrogram during t would display nuclear fluctuations that do not depend on the history of the distinct exciton during τ. However, a dependence on this history reveals that the nuclear environments are correlated.

The Microscopic Origin of Spectral Fluctuations

Before interaction with light, the sample ensemble begins in an equilibrium distribution determined by its temperature. At 77 K (k_BT = 54 cm^{-1}), only the electronic

ground state is significantly populated, and its vibrational sub-levels above approximately 110 cm^{-1} are negligibly populated in a Bose-Einstein distribution. Nonetheless, the ensemble contains a variety of nuclear configurations at equilibrium. Furthermore, we assume that the dynamics of distinct proteins are independent of each other, within a time domain.

For each excited state, the ensemble is excited to a distribution of Franck-Condon frequencies because of its variety of nuclear configurations at equilibrium. However, under the conditions specified previously, the signal is subject to the central limit theorem. Each pulse interacts with 10^{10} proteins, integrated over approximately 5,000 experiments per parametrization of τ and T. Despite the diversity of Franck-Condon frequencies, both initially and over time, the peaks in the spectrograms are narrowed toward the time-dependent ensemble average by the central limit theorem. As a result, because the same set of vibrational modes is shared across the ensemble, the mean of their signal frequencies fluctuates over time; and their peak position will also shift to accommodate this underlying moving average. As discussed below and in Sections S6 and S12 of the Supplemental Information, the spectral fluctuation amplitudes are further reduced by the choice of short-time Fourier-transform window.

Signal Processing

The 2D experiment yields a three-dimensional dataset depending on τ, T, and t according to the third-order response function shown in Equation 1.

$$S^{(3)}(\tau,T,t)=\left(\frac{i}{\hbar}\right)^3\theta(\tau)\theta(T)\theta(t)\sum\nolimits_{\alpha=1}^{4}R_\alpha(\tau,T,t)-R_\alpha^*(\tau,T,t) \qquad \text{(Equation 1)}$$

Here, $\theta(t)$ are Heaviside step functions with an onset at t, and $R_\alpha(\tau,T,t)$ refers to the contributions from four distinct Liouville pathways available under the rotating wave approximation (Equation 2). In these equations, a, b, c, and d represent states, $P(a)$ is the probability of occupying state a, and μ_{ab} are the transition dipoles between states a and b.

$$\begin{aligned}
R_1(\tau,T,t)&=\sum_{a,b,c,d}P(a)\mu_{ab}\mu_{bc}\mu_{cd}\mu_{da}\exp\left(i[\omega_{d,a}\tau+\omega_{d,b}T+\omega_{d,c}t]\right)\\
R_2(\tau,T,t)&=\sum_{a,b,c,d}P(a)\mu_{ab}\mu_{bc}\mu_{cd}\mu_{da}\exp\left(i[\omega_{a,b}\tau+\omega_{d,b}T+\omega_{d,c}t]\right)\\
R_3(\tau,T,t)&=\sum_{a,b,c,d}P(a)\mu_{ab}\mu_{bc}\mu_{cd}\mu_{da}\exp\left(i[\omega_{a,b}\tau+\omega_{a,c}T+\omega_{d,c}t]\right)\\
R_4(\tau,T,t)&=\sum_{a,b,c,d}P(a)\mu_{ab}\mu_{bc}\mu_{cd}\mu_{da}\exp\left(i[\omega_{d,a}\tau+\omega_{c,a}T+\omega_{b,a}t]\right)
\end{aligned} \qquad \text{(Equation 2)}$$

Equation 2 yields a signal that oscillates in each of the time domains, and the Fourier-transform operation interconverts between the time and frequency domains. For reference, if the three-dimensional dataset is initially represented entirely in the time domain, standard 2D spectra are obtained by Fourier transform over τ and t (Figure S1).

In 2D-STEPS, one-dimensional time series (along τ) are selected at ω_t, corresponding to the frequency of a given exciton. As described above, these time series are damped sinusoidal curves (see Figures S2 and S3), each of which propagates at the frequency $\omega_{ei,g}$ for exciton i. The damping is due to excitonic frequency fluctuations arising from environmental perturbations after excitation to the Franck-Condon region.[7] Using the short-time Fourier-transform technique, we extracted ensemble-averaged trajectories of the spectral motion at regions of the data along the τ domain by sliding a 140 fs (fwhm) Hanning window $U(\tau+\tau')$ along the

τ dimension through variation of τ' and performing a Fourier transform at each step to populate the rows of the spectrogram (Equation 3). (For other window widths, see Figures S4 and S5 for FMO and S12 for Nile Blue A.)

$$A_{2D-STEPS}(\tau', \omega'_\tau, \omega_t) = \sum_T \left| F_\tau \left[U(\tau + \tau') S^{(3)}(\tau, T, \omega_t) \right] \right| \quad \text{(Equation 3)}$$

Here, τ' is the lag in coherence time specified at the central window position, and $\mathscr{F}_\tau[f(\tau)]$ denotes Fourier transform of the specified function $f(\tau)$ with respect to τ. For a 140 fs (fwhm) window width, the first data point is at $\tau' = 140$ fs, because this is the position where the one edge of the window is at $\tau = 0$ fs. If the edge of the window is allowed to extend to negative τ, then non-rephasing contributions leak into the resulting spectra and complicate the analysis. To avoid complications of the phase arising from the spectrograms, the absolute values were taken. Subsequently, for 2D-STEPS of FMO they were summed in the T domain. For further discussion justifying this approach, see Section S5 in the Supplemental Information. Applying the short-time Fourier transform along τ generates two-dimensional spectrograms in τ' versus ω'_τ, where ω'_τ is the spectrum of the signal within the moving time window. For clarity, the prime marks indicate correspondence of a given parameter to a window of data, rather than across the full time series. Whereas spectrograms obtained along τ are shown in Figure 2, those obtained along t are shown for reference in Figure S9.

In 2D-TRIPS, the methods are similar to those of 2D-STEPS; however, window functions are applied in both the τ and t domains, and because of time-ordering considerations, particular values of T are specified rather than summed (Equations 4 and 5). Here, t' is the lag time in the rephasing domain.

$$A_{2D-TRIPS}(\tau', \omega'_\tau, T, t', \omega'_t) = \left| F_t \left[U(t + t') S_F^{(3)}(\tau', \omega'_\tau, T, t) \right] \right| \quad \text{(Equation 4)}$$

$$S_F^{(3)}(\tau', \omega'_\tau, T, t) = F_\tau \left[U(\tau + \tau') S^{(3)}(\tau, T, t) \right] \quad \text{(Equation 5)}$$

We use these datasets to investigate the dependence of ω'_τ on the τ' and t' dimensions.

SUPPLEMENTAL INFORMATION

Supplemental Information includes Supplemental Experimental Procedures, 15 figures, and 1 table and can be found with this article online at https://doi.org/10.1016/j.chempr.2017.12.009.

ACKNOWLEDGMENTS

B.S.R., H.Z., V.P.S., P.N., A.R.G., J.R.C., and G.S.E. would like to thank the Materials Research Science and Engineering Centers (DMR 14- 20709), the Air Force Office of Scientific Research (grant no. FA9550-14-1-0367), the Department of Defense Vannevar Bush Fellowship (grant no. N00014-16-1-2513), the Camille and Henry Dreyfus Foundation, and the Sloan Foundation for partially supporting the work in this publication. K.A., A.T.G., and R.J.C. gratefully acknowledge funding from the Photosynthetic Antenna Research Center, an Energy Frontier Research Center funded by the Basic Energy Sciences program of the US Department of Energy Office of Science, under award no. DE-SC0001035. S.K. and S.-H.Y. were supported by Qatar National Research Fund exceptional grant NPRPX-107-1-027.

AUTHOR CONTRIBUTIONS

B.S.R., H.Z., P.N., A.R.G., and J.R.C. performed the experiments. S.-H.Y. and S.K. performed the simulations. B.S.R., V.P.S., S.-H.Y., and G.S.E. analyzed and

interpreted the data. K.A., A.T.G., and R.J.C. purified the sample. All authors contributed to the manuscript. G.S.E., S.K., and R.J.C. supervised the project.

DECLARATION OF INTERESTS

The authors declare no competing interests.

Received: May 16, 2017
Revised: September 5, 2017
Accepted: December 14, 2017
Published: January 11, 2018

REFERENCES AND NOTES

1. Vasmel, H., van Dorssen, R.J., de Vos, G.J., and Amesz, J. (1986). Pigment organization and energy transfer in the green photosynthetic bacterium *Chloroflexus aurantiacus*: I. The cytoplasmic membrane. Photosynth. Res. *7*, 281–294.

2. Rebentrost, P., Mohseni, M., Kassal, I., Lloyd, S., and Aspuru-Guzik, A. (2009). Environment-assisted quantum transport. New J. Phys. *11*, 033003.

3. Abramavicius, D., and Valkunas, L. (2016). Role of coherent vibrations in energy transfer and conversion in photosynthetic pigment–protein complexes. Photosynth. Res. *127*, 33–47.

4. Chenu, A., Christensson, N., Kauffmann, H.F., and Mančal, T. (2013). Enhancement of vibronic and ground-state vibrational coherences in 2D spectra of photosynthetic complexes. Sci. Rep. *3*, https://doi.org/10.1038/srep02029.

5. Ishizaki, A., Calhoun, T.R., Schlau-Cohen, G.S., and Fleming, G.R. (2010). Quantum coherence and its interplay with protein environments in photosynthetic electronic energy transfer. Phys. Chem. Chem. Phys. *12*, 7319.

6. Chen, X., and Silbey, R.J. (2011). Excitation energy transfer in a non-markovian dynamical disordered environment: localization, narrowing, and transfer efficiency. J. Phys. Chem. B *115*, 5499–5509.

7. Mukamel, S. (1995). Principles of Nonlinear Optical Spectroscopy (Oxford University Press).

8. Ladd, T.D., Jelezko, F., Laflamme, R., Nakamura, Y., Monroe, C., and O'Brien, J.L. (2010). Quantum computers. Nature *464*, 45–53.

9. Panitchayangkoon, G., Hayes, D., Fransted, K.A., Caram, J.R., Harel, E., Wen, J., Blankenship, R.E., and Engel, G.S. (2010). Long-lived quantum coherence in photosynthetic complexes at physiological temperature. Proc. Natl. Acad. Sci. USA *107*, 12766–12770.

10. Lee, H., Cheng, Y.C., and Fleming, G.R. (2007). Coherence dynamics in photosynthesis: protein protection of excitonic coherence. Science *316*, 1462–1465.

11. Savikhin, S., and Struve, W.S. (1994). Ultrafast energy transfer in FMO trimers from the green bacterium *Chlorobium tepidum*. Biochemistry *33*, 11200–11208.

12. Engel, G.S., Calhoun, T.R., Read, E.L., Ahn, T.-K., Mancal, T.s., Cheng, Y.-C., Blankenship, R.E., and Fleming, G.R. (2007). Evidence for wavelike energy transfer through quantum coherence in photosynthetic systems. Nature *446*, 782–786.

13. Fidler, A.F., Caram, J.R., Hayes, D., and Engel, G.S. (2012). Towards a coherent picture of excitonic coherence in the Fenna–Matthews–Olson complex. J. Phys. B Mol. Opt. Phys. *45*, 154013.

14. Plenio, M.B., and Huelga, S.F. (2008). Dephasing-assisted transport: quantum networks and biomolecules. New J. Phys. *10*, 113019.

15. Mohseni, M., Rebentrost, P., Lloyd, S., and Aspuru-Guzik, A. (2008). Environment-assisted quantum walks in photosynthetic energy transfer. J. Chem. Phys. *129*, 174106.

16. Ishizaki, A., and Fleming, G.R. (2009). Theoretical examination of quantum coherence in a photosynthetic system at physiological temperature. Proc. Natl. Acad. Sci. USA *106*, 17255–17260.

17. Tempelaar, R., Jansen, T.L.C., and Knoester, J. (2014). Vibrational beatings conceal evidence of electronic coherence in the FMO light-harvesting complex. J. Phys. Chem. B *118*, 12865–12872.

18. Plenio, M.B., Almeida, J., and Huelga, S.F. (2013). Origin of long-lived oscillations in 2D-spectra of a quantum vibronic model: electronic versus vibrational coherence. J. Chem. Phys. *139*, 235102.

19. Tiwari, V., Peters, W.K., and Jonas, D.M. (2013). Electronic resonance with anticorrelated pigment vibrations drives photosynthetic energy transfer outside the adiabatic framework. Proc. Natl. Acad. Sci. USA *110*, 1203–1208.

20. Christensson, N., Kauffmann, H.F., Pullerits, T., and Mančal, T. (2012). Origin of long-lived coherences in light-harvesting complexes. J. Phys. Chem. B *116*, 7449–7454.

21. Caram, J.R., Lewis, N.H.C., Fidler, A.F., and Engel, G.S. (2012). Signatures of correlated excitonic dynamics in two-dimensional spectroscopy of the Fenna-Matthew-Olson photosynthetic complex. J. Chem. Phys. *136*, 104505.

22. Singh, V.P., Westberg, M., Wang, C., Dahlberg, P.D., Gellen, T., Gardiner, A.T., Cogdell, R.J., and Engel, G.S. (2015). Towards quantification of vibronic coupling in photosynthetic antenna complexes. J. Chem. Phys. *142*, 212446.

23. Hayes, D., Wen, J., Panitchayangkoon, G., Blankenship, R.E., and Engel, G.S. (2011). Robustness of electronic coherence in the Fenna–Matthews–Olson complex to vibronic and structural modifications. Faraday Discuss. *150*, 459–469.

24. Abramavicius, D., and Mukamel, S. (2011). Exciton dynamics in chromophore aggregates with correlated environment fluctuations. J. Chem. Phys. *134*, 174504.

25. Caycedo-Soler, F., Chin, A.W., Almeida, J., Huelga, S.F., and Plenio, M.B. (2012). The nature of the low energy band of the Fenna-Matthews-Olson complex: vibronic signatures. J. Chem. Phys. *136*, 155102.

26. Wu, J., Liu, F., Ma, J., Silbey, R.J., and Cao, J. (2012). Efficient energy transfer in light-harvesting systems: quantum-classical comparison, flux network, and robustness analysis. J. Chem. Phys. *137*, 174111.

27. Silbey, R. (1976). Electronic energy transfer in molecular crystals. Annu. Rev. Phys. Chem. *27*, 203–223.

28. Tronrud, D.E., Wen, J., Gay, L., and Blankenship, R.E. (2009). The structural basis for the difference in absorbance spectra for the FMO antenna protein from various green sulfur bacteria. Photosynth. Res. *100*, 79–87.

29. Hayes, D., and Engel, G.S. (2011). Extracting the excitonic hamiltonian of the Fenna-Matthews-Olson complex using three-dimensional third-order electronic spectroscopy. Biophys. J. *100*, 2043–2052.

30. Rätsep, M., and Freiberg, A. (2007). Electron–phonon and vibronic couplings in the FMO bacteriochlorophyll a antenna complex studied by difference fluorescence line narrowing. J. Lumin. *127*, 251–259.

31. Lee, M.K., and Coker, D.F. (2016). Modeling electronic-nuclear interactions for excitation energy transfer processes in light-harvesting complexes. J. Phys. Chem. Lett. *7*, 3171–3178.

32. Matsuzaki, S., Zazubovich, V., Rätsep, M., Hayes, J.M., and Small, G.J. (2000). Energy transfer kinetics and low energy vibrational structure of the three lowest energy qy-states of the Fenna-Matthews-Olson antenna complex. J. Phys. Chem. B *104*, 9564–9572.

33. Czarnecki, K., Diers, J.R., Cynwat, V., Erickson, J.P., Frank, H.A., and Bocian, D.F. (1997). Characterization of the strongly coupled, low-frequency vibrational modes of the special pair of photosynthetic reaction centers via isotopic labeling of the cofactors. J. Am. Chem. Soc. *119*, 415–426.

34. Schulze, J., and Kühn, O. (2015). Explicit correlated exciton-vibrational dynamics of the FMO complex. J. Phys. Chem. B *119*, 6211–6216.

35. Fearey, B.L., Carter, T.P., and Small, G.J. (1983). Efficient nonphotochemical hole burning of dye molecules in polymers. J. Phys. Chem. *87*, 3590–3592.

36. Miller, S.K., Baiker, A., Meier, M., and Wokaun, A. (1984). Surface-enhanced Raman scattering and the preparation of copper substrates for catalytic studies. J. Chem. Soc. Faraday Trans. 1 *80*, 1305–1310.

37. Zhang, Y., Hartmann, S.R., and Moshary, F. (1996). Fluorescence-line-narrowing spectroscopy of nile blue in glass and polymer at 5 K: determination of a single-site line shape function. J. Chem. Phys. *104*, 4371–4379.

38. Le Ru, E.C., Schroeter, L.C., and Etchegoin, P.G. (2012). Direct measurement of resonance Raman spectra and cross sections by a polarization difference technique. Anal. Chem. *84*, 5074–5079.

39. Cho, M., Vaswani, H.M., Brixner, T., Stenger, J., and Fleming, G.R. (2005). Exciton analysis in 2D electronic spectroscopy. J. Phys. Chem. B *109*, 10542–10556.

40. Cina, J.A., Kovac, P.A., Jumper, C.C., Dean, J.C., and Scholes, G.D. (2016). Ultrafast transient absorption revisited: phase-flips, spectral fingers, and other dynamical features. J. Chem. Phys. *144*, 175102–175119.

41. Nazir, A. (2009). Correlation-dependent coherent to incoherent transitions in resonant energy transfer dynamics. Phys. Rev. Lett. *103*, 146404.

42. Kuramoto, Y. (1984). Chemical Oscillations, Waves, and Turbulence (Springer).

43. Strogatz, S.H. (2000). From Kuramoto to Crawford: exploring the onset of synchronization in populations of coupled oscillators. Physica D *143*, 1–20.

44. Rebentrost, P., Mohseni, M., and Aspuru-Guzik, A. (2009). Role of quantum coherence and environmental fluctuations in chromophoric energy transport. J. Phys. Chem. B *113*, 9942–9947.

45. Löhner, A., Ashraf, K., Cogdell, R.J., and Köhler, J. (2016). Fluorescence-excitation and emission spectroscopy on single FMO complexes. Sci. Rep. *6*, https://doi.org/10.1038/srep31875.

46. Zheng, H., Caram, J.R., Dahlberg, P.D., Rolczynski, B.S., Viswanathan, S., Dolzhnikov, D.S., Khadivi, A., Talapin, D.V., and Engel, G.S. (2014). Dispersion-free continuum two-dimensional electronic spectrometer. Appl. Opt. *53*, 1909.

47. Turner, D.B., Dinshaw, R., Lee, K.-K., Belsley, M.S., Wilk, K.E., Curmi, P.M.G., and Scholes, G.D. (2012). Quantitative investigations of quantum coherence for a light-harvesting protein at conditions simulating photosynthesis. Phys. Chem. Chem. Phys. *14*, 4857–4874.

48. Wang, L., Griffin, G.B., Zhang, A., Zhai, F., Williams, N.E., Jordan, R.F., and Engel, G.S. (2017). Controlling quantum-beating signals in 2D electronic spectra by packing synthetic heterodimers on single-walled carbon nanotubes. Nat. Chem. *9*, 219–225.